Dynamic Model of Commercially Available Inverters with Validation Against Hardware Testing

Panagiotis Bountouris, Dimitrios Tzelepis, *Member, IEEE*, Ibrahim Abdulhadi, *Member, IEEE*, Federico Coffele, *Member, IEEE*

***Abstract*—The increasing penetration of photovoltaics (PV) in the bulk power system has led to the growing need for better understanding the behavior of PV inverters during grid disturbances. A configurable dynamic model is presented in this paper emulating the behavior of a Low Voltage (LV) connected off-the-shelf PV inverter during faults and voltage dips. The model has been developed and validated against the results acquired throughout the empirical characterization of the real inverter. The physical testing of the Device Under Test (DUT) was performed at the Power Networks Demonstration Centre (PNDC), where the required network conditions were applied at the output of the inverter using a Real Time Digital Simulator (RTDS). Further simulations, conducted with the aid of the developed model, aim to reflect a distribution network dominated by inverter connected generation under a number of imposed fault scenarios.**

***Index Terms*—PV inverter physical testing, dynamic inverter model, distribution network, low voltage, average model.**

I. Introduction

THE widespread penetration of renewable energy sources (RES) is driven by the carbon reductions objectives and the net zero target by 2050 [1]. This trend poses increasingly higher challenges to distribution system operators (DSOs) in preserving quality and continuity of supply. On top of that, the evident inconsistencies in inverter operation across LV-connected PV inverters of various manufacturers indicate the risk of invalid assumptions when system studies are conducted [2, 3, 4, 5].

A growing number of bench testing studies reported in the literature examine LV grid-tied PV inverters behavior against grid disturbances, which can potentially affect their response and connection stability. A Loss of Mains (LoM) oriented hardware based study [2] evaluated the PV inverters' grid connection stability during frequency and voltage phase shift events. The DUTs performed similarly with regards to sensitivity and stability during the applied scenarios however, discrepancies were noticed at their active and reactive power output. In addition, several off-the-shelf LV-connected PV inverters of different manufacturers exhibited a wide range of behaviors in [3] and [4], when experimentally tested under faults and voltage disturbances. The results of [5] validate the aforementioned concerns regarding the inverters' operation inconsistency during faults. In the particular study, the same small scale PV inverters with those in [3] were tested under voltage magnitude and vector shift (VS) variations imposed on their LV terminals.

Moreover, the literature has reported a number of studies that attempted to reflect the response of PV inverters during fault conditions with the aid of simulation models [6, 7, 8, 9, 10, 11, 12, 13, 14, 15, 16, 17, 18, 19, 20, 21, 22, 23, 24]. Authors in [6, 7, 8, 9, 10, 11, 12] presented detailed models emulating PV inverters under fault conditions, although the latter were not validated against hardware testing. The modeling work of [6] focuses on the initial fault response of inverter based generation, meaning the peak current during the sub-transient period, neglecting the transient period and steady-state behavior. Authors in [12] claim that electromagnetic transient simulations are appropriate when considering sub-cycle dynamic analysis and inverter switching dynamics.

The bench testing results of [16] and [17] were implemented to validate inverter models for power system dynamic studies. The inverter model presented in [16] operated only at 1 p.u. pre-fault loading level of inverter rating. Models in [13] and [21] are also compared against grid connected inverters. However, the hardware based characterization in [13] is not realized through exhausting physical testing. In addition, authors in [21] do not provide detailed information with regards to the inverter modelling methodology and structure. The mathematical model in [18] is validated against an existing real life PV power plant, although its dynamic behaviour against fault conditions is not examined. Useful insights are given in [19], which compares the dynamic behavior of different inverter models during fault scenarios against commercial inverters. Furthermore, General Electric (GE) [25], Electric Power Research Institute (EPRI) [26] and the Western Electricity Coordinating Council (WECC) [27, 28] provide guidelines for the development of generic dynamic simulation models emulating transmission connected PV inverters or distribution installed PV plants. However, this approach cannot be inherited for individual small scale PV inverters due to the variation of responses among different manufacturers during fault conditions.

Therefore, the noted lack of dynamic modeling schemes accurately emulating LV-connected PV inverters of various manufacturers, due to the observed inconsistency among the latter, highlights the need of further investigation. This paper presents the development and hardware-based validation of a novel dynamic model which is tuned in order to emulate the fault response of a particular commercially available PV

[1]This project was funded under the core research program contributed by the members of the University of Strathclyde's PNDC (http://pndc.co.uk/).

[2]P. Bountouris and D. Tzelepis are with the Department of Electronic and Electrical Engineering, University of Strathclyde, Glasgow, G1 1XW, U.K.

[3]I. Abdulhadi and F. Coffele are with the Power Networks Demonstration Centre, University of Strathclyde, Glasgow, G68 0EF, U.K.

This is a peer reviewed, accepted author manuscript of the following research article: Bountouris, P., Tzelepis, D., Abdulhadi, I., & Coffele, F. (2022). Dynamic model of commercially available inverters with validation against hardware testing. IEEE Transactions on Power Systems. https://doi.org/10.1109/TPWRS.2022.3179667

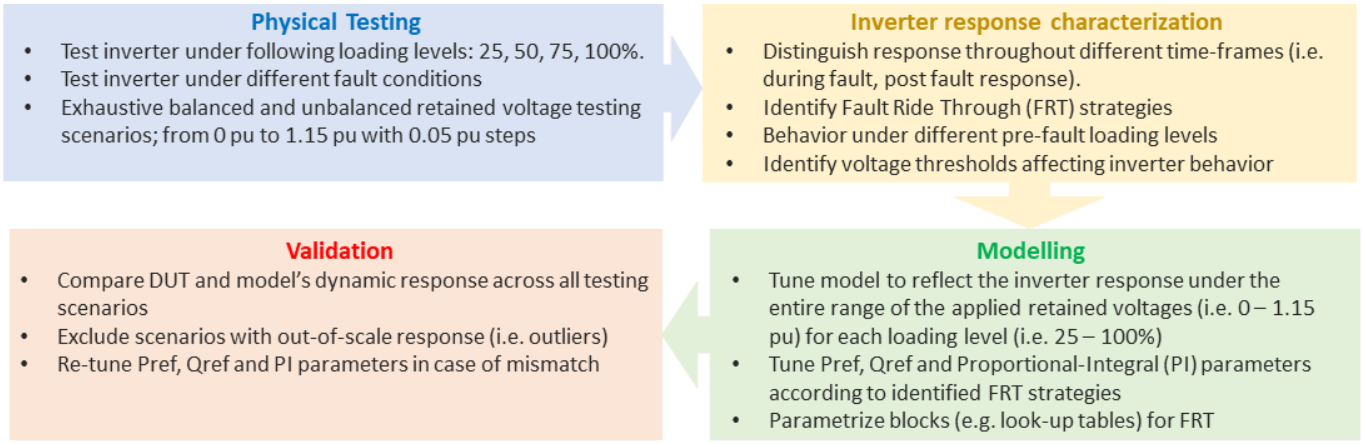

Fig. 1. Overview of the developed methodology.

inverter. This is an RMS average model which is based on sinusoidal current source injection omitting the effects of semiconductor switching. The paper proposes a complete methodology, including physical testing, modeling, simulations and validation. It shall be noted that the proposed methodology and model structure are deployable to validate any converter of this scale. The model itself may be informed and tuned based on the guidelines described within the framework, in conjunction with the testing scenarios and functions of interest (i.e. FRT).

Firstly the physical testing set up and results of a three-phase photovoltaic inverter is presented in Section II. The hardware level testing focused on the characterization of the inverter's behavior during network faults and voltage disturbances. Section III describes the main structure and the control scheme of the developed dynamic model emulating the response of a specific commercial PV inverter under the implemented physical testing conditions. The performance of the dynamic model is validated against the recorded current output of the real inverter when tested in PNDC facilities [29]. Finally, the PV inverter model is integrated at multiple points of the LV part of a simulated distribution network and asymmetrical faults are applied at the Medium Voltage (MV) side.

A. Methodology

Fig. 1 presents the methodology proposed througout this paper in order to accomplish accurate emulation of small scale commercial PV inverters. In particular the steps from the real inverter physical testing to the development and validation of the dynamic model are clearly listed and can be followed for modeling inverters of different manufacturers. The proposed structure and adjustable parameters (i.e. PI gains, Pref and Qref) constitute the model flexible to reflect the behavior of different inverter types.

1) Physical testing: The experimental testing is an important task supporting both tuning and validation of the model. The inverter is examined under a wide range of voltage scenarios and fault conditions while loaded with different levels (i.e. 25, 50, 75, 100%). This step is an essential requirement in order to achieve empirical characterization of the actual inverter.

2) Inverter response characterisation: The results extracted during physical testing provide valuable information in order to effectively characterize the fault response of the inverter throughout the various time frames (i.e. during fault, post fault period) of the imposed events. Moreover, this task will enable the identification of the available inverter FRT or Low Voltage Ride Through (LVRT) strategy and the network conditions, such as thresholds of voltage depression, which lead the inverter to the activation of such functions.

3) Modelling: The results acquired throughout testing and the empirical characterization of the inverter enable wise tuning of the model. The aim is to accurately reflect the identified FRT response of the real device by adjusting the Pref, Qref and PI parameters depending on the network conditions identified during the previous task (i.e. voltage depression thresholds). It shall be noted that for the tuninig exercise, depending on the application and requriements, it would be beneficial to deploy sophisticated methods to allow auto- and adaptive tuning. This is anticipated to introduce certain benefits accounting for minimization of tuning effort, elimitation of potential instabilities and improvement of transient performance [30, 31].

4) Validation: Validation of the model is accomplished by comparing its output current against this of the real inverter under test, while simulating all physical testing scenarios. Corrective re-tuning of the model is recommended in case of major discripancies, however scenarios with out-of-scale response should be omitted.

II. PV INVERTER PHYSICAL TESTING

The development of the model is based on the physical testing of a three phase LV PV inverter rated at 60 kVA. The inverter under test is an off-the-shelf product following the GB ENA Engineering Recommendation G59/3 and the relevant FRT requirements which are defined in the GB Grid Code [32, 33]. The objective of the experimental investigation is to characterize the output and hence the response of the inverter during the imposed conditions. The inverters under test were subject to various voltage profiles, reflecting different conditions of the grid. The following factors were considered throughout the numerous testing scenarios:

- Voltage magnitude at inverter's output

- Inverter loading prior to the fault/voltage disturbance
- Voltage point on wave (PoW) at fault inception

A. Test setup

The test setup shown in Fig. 2 was implemented to apply LV voltage disturbances and fault conditions at the output of the PV inverter, with the aid of RTDS [34] and Triphase [35]. The latter is a configurable power-electronics based device which can operate either as a (AC or DC) voltage or current source. For this testing, Triphase was configured as a 3-phase AC voltage source and it was able to sink the currents produced by the PV inverter. Its voltage output can be controlled through voltage set-points provided by RTDS. In particular, The AC network conditions are simulated in RTDS and the resulting voltage profiles at the position of tinterest, have been extracted and applied to the inverter under-test via the Triphase unit. The Aurora link has been used to transfer the numerical values of voltage from the RTDS to Triphase. Effectively, the Triphase unit was utilized as a means to impose the network conditions to the inverter under-test.

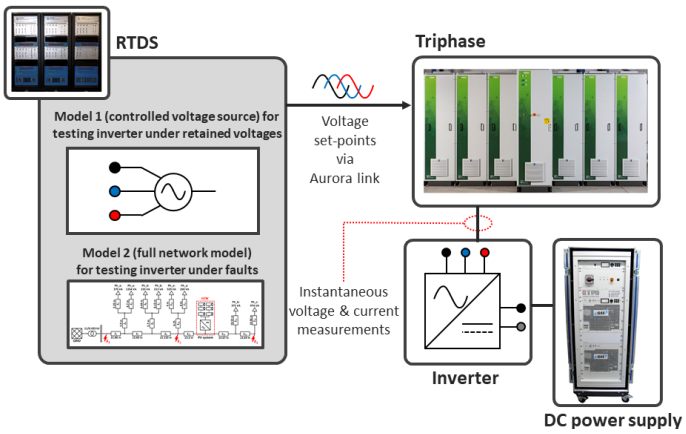

Fig. 2. Test network setup for voltage disturbance testing and faults.

The PV inverter was supplied by a PV emulator [36] rated at 64 kW maximum power and 1000 V maximum DC voltage. The particular equipment allowed to examine the DUT under a wide range of loading levels (25-100%). Moreover, a monitoring system based on Beckhoff analogue acquisition cards was deployed to acquire the instantaneous voltage and current measurements at the output of the PV inverter. The reporting rate was set at 5 kHz, although the terminal of the referred measuring device is able to measure at significantly shorter intervals through oversampling with maximum measuring error of $\pm 0.5\%$ relative to the full scale value ($U_{L\text{-}L}$max.:500V, $U_{L\text{-}N}$max.:288V, U_{DC}max.:410V) [37]. It is highlighted that, the inverter modelling exercise will be based on the data extracted during the physical testing. The time-step of 0.2 ms corresponding to the referred sampling frequency, is considered sufficient for the required modelling simulations according to [38, 39].

During the laboratory assessment, the voltage at the terminals of the PV inverter was determined by the simulated AC conditions in RTDS. This was achieved via two ways. First, voltage disturbances were artificially applied with the aid of a fully controllable three-phase voltage source (Model 1). By this way, the inverter was tested under a wide range of predetermined balance and unbalanced AC network voltage scenarios, which are reported in Table I.

TABLE I
VOLTAGE DISTURBANCES TEST SCHEDULE

Loading (%)	***Balanced Retained Voltage*** *(pu)*		
25, 50, 75, 100	0 - 1.15 (with step of 0.05)		
Loading (%)	***Retained Phase Voltages*** *(pu)*		
	Va	Vb	Vc
25, 50, 75, 100	1	1	0
	1	1	0.25
	1	1	0.5
	1	1	0.75
	1	1	1.15
	1	0	0
	1	0.25	0.25
	1	0.5	0.5
	1	0.75	0.75
	1	1.15	1.15
	1	0	1.15
	1	0.25	0.75
	1	0.75	0.25
	1	1.15	0

In addition, fault conditions were created via a second RSCAD model (Model 2) representing a real LV distribution network, using parameters published by Electricity North West [40]. Thus, the inverter is also examined under a wide range of voltage depressions caused by different fault types, fault locations and PoW scenarios. With respect to voltage PoW, it shall be noted that depending on the voltage value upon the fault inception, different signatures may be observed at the converter terminals accounting for voltages and currents. Additionally, since most of the converter controls are based on PLL elements, PoW has been found to have an impact on the ability of inverters to stay synchronized to the main grid [41, 42]. Even PoW is not the main focus of this work, due to its potential impact on the inverter behaviour, several PoW scenarios have been considered in the tests. Table II lists the implemented fault cases. Fault period of 300 ms is considered a typical fault duration given the fact that the fault clearance time ranges among 100 – 400 ms, depending on the protection zone. Fig. 3 depicts the AC network topology modeled in the RTDS, indicating the point of connection of the PV inverter hardware (H/W). The same single-line-diagram (SLD) includes the cable feeder lengths, the LV loads per phase, the MV/LV step-down transformer as well as the locations of the applied faults (F_1, F_2 and F_3). Detailed information the LV feeders impedance is provided in Table III.

B. Testing observations and discussion

It has been observed throughout testing that voltage dips usually result in an immediate response of the PV inverters with a current peak of short duration, which is caused by the

TABLE II
FAULT SCENARIOS

Fault location	*Fault type*	*Fault resistance* (Ω)	*Voltage PoW* ($^\circ$)	*Fault duration* (ms)
F1, F2, F3	p-g, p-p, p-p-g, 3-p-g	0, 0.1	0, 90	300

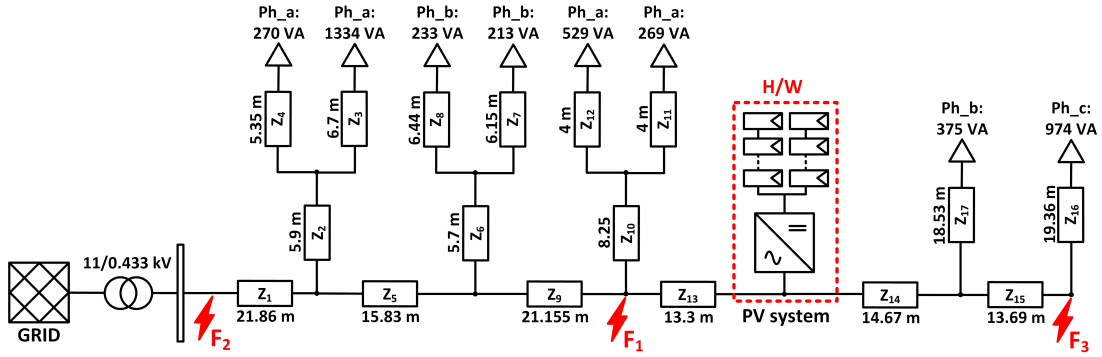

Fig. 3. LV AC network modeled in RSCAD.

TABLE III
LV FEEDERS CHARACTERISTICS

Feeder section	*R* ($m\Omega$)	*X* ($m\Omega$)	R_0 ($m\Omega$)	X_0 ($m\Omega$)
Z_1	9.75	1.55206	32.8993	1.81438
Z_2	6.785	0.5192	32.8993	0.5192
Z_3	7.705	0.5896	8.04	0.5896
Z_4	6.1525	0.4708	6.42	0.4708
Z_5	7.06018	1.12393	23.82415	1.31389
Z_6	6.555	0.5016	6.84	0.5016
Z_7	7.073	0.5412	7.38	0.5412
Z_8	7.406	0.56672	7.728	0.56672
Z_9	9.43513	1.502005	31.838275	1.755865
Z_{10}	9.4875	0.726	9.9	0.726
Z_{11}	4.6	0.352	4.8	0.352
Z_{12}	4.6	0.352	4.8	0.352
Z_{13}	5.9318	0.9443	20.0165	1.1039
Z_{14}	1.30563	0.990225	4.67973	1.11492
Z_{15}	1.21841	0.924075	4.36711	1.04044
Z_{16}	22.264	1.70368	23.232	1.70368
Z_{17}	21.3095	1.63064	22.236	1.63064

output filter. Then, depending on the level of voltage depression, current control is required to prevent the inverter from potential thermal overload. This kind of behavior differentiates it of that of a conventional electrical generator.

Moreover, two distinct current behaviors have been noted during faults (or voltage disturbances), referred in this paper as FRT 1 and FRT 2. During FRT 1, the inverter increases its current output within admissible thermal limits while providing reactive power to support the voltage at the AC side. When a more severe voltage depression is applied, exceeding certain thresholds, the inverter operates in FRT 2 mode. In this case the device immediately stops feeding in current, in an attempt to remain connected throughout the event period (voltage disturbance, fault). After the event is cleared, the AC output current gradually increases to reach the pre-fault level.

1) Fault conditions: Fig. 4 and Fig. 5 depict the FRT 1 and FRT 2 operation modes of the 60 kVA inverter under slightly different conditions. In both cases, the DUT was 100% loaded and a phase-to-ground fault at location F_1 is applied. The fault introduced in the first scenario depicted at Fig. 4 is resistive (0.1 Ω) and initiated at 0° PoW. During this case the inverter followed the FRT 1 strategy. On the other hand, Fig. 5 shows measurements captured during a solid fault applied at 90° PoW. The mentioned conditions lead the inverter to FRT 2 operation.

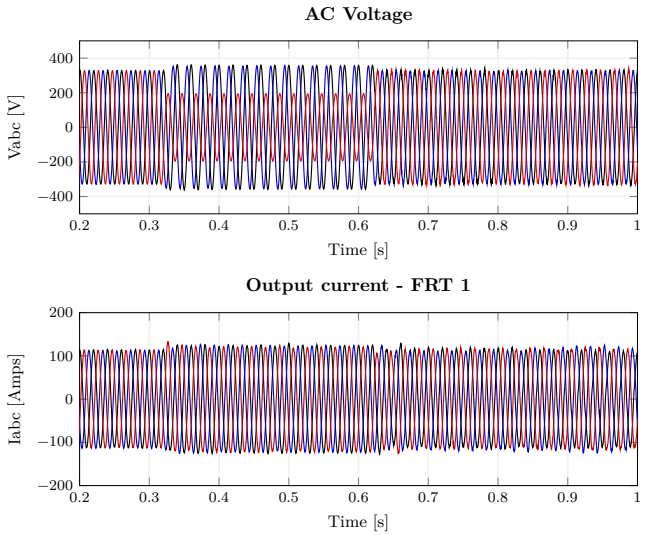

Fig. 4. 100% Loading – Fault response test (phase-to-ground, fault location 1, 0° PoW, 0.1 Ω) - FRT 1.

2) Voltage disturbances: Throughout the analysis, it was noted that depending on the loading level, the inverter exhibits different FRT responses for the same voltage disturbances. For instance, Fig. 6 and Fig. 7 present the response of the inverter under a balanced voltage depression of 0.6 pu, when the DUT was loaded with 25% and 75% of maximum power respectively. The inverter exhibited an FRT 1 response during the first case, as it was lightly loaded and so there was no risk to exceed inverter thermal overload thresholds. That is not the case for the second testing scenario where the DUT's loading is 75% and therefore the device activates FRT 2 strategy aiming to retain its grid connection stability.

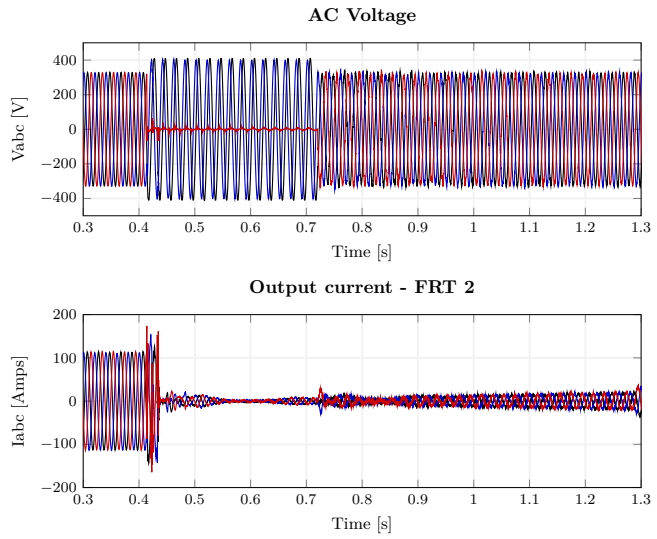

Fig. 5. 100% Loading – Fault response test (phase-to-ground, fault location 1, 90° PoW, 0 Ω) - FRT 2.

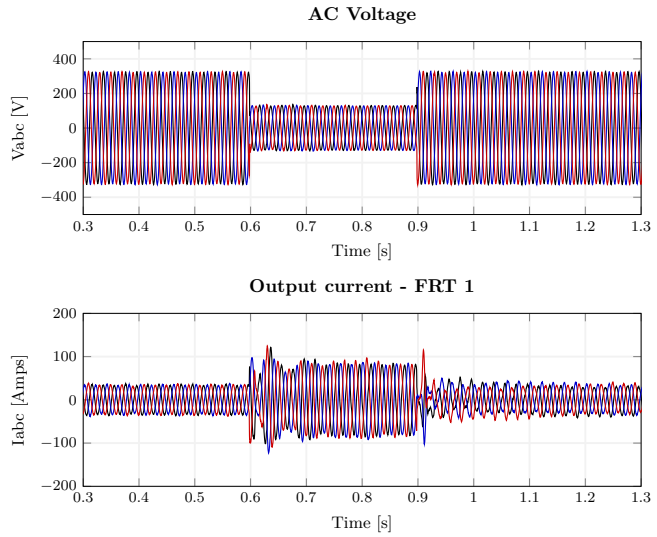

Fig. 6. 25% Loading – 0.4 pu retained balanced voltage – FRT 1.

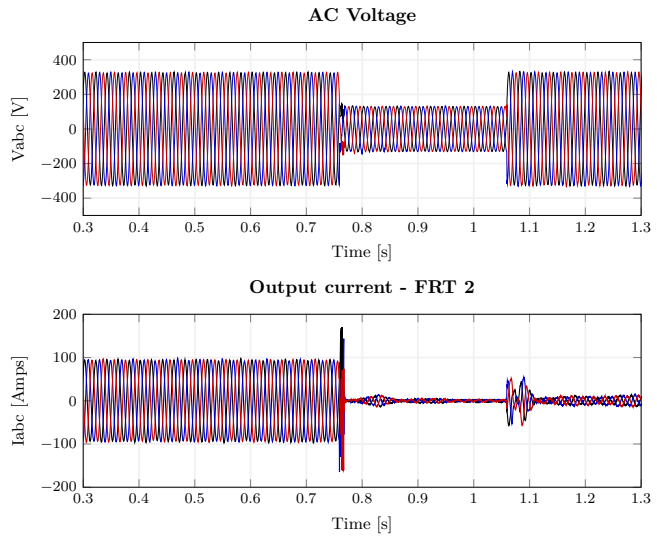

Fig. 7. 75% Loading – 0.4 pu retained balanced voltage – FRT 2.

III. Inverter Modelling & Validation

In this section, the main structure and parameters of the developed inverter model are presented. The latter is built with the aid of MATLAB Simulink. It involves a number of control stages that determine the behavior of the inverter depending on the network voltage conditions and the loading level of the device. The control architecture is based on that recommended by the Renewable Energy Modeling Task Force of the WECC [43], but significantly modified as the latter incorporates large scale PV plants control schemes (i.e. V/Q and frequency control).

Initially, the data extracted during the physical testing were used to observe and characterize the FRT behavior of the real inverter, as described in the previous section. This exercise aided the model tuning in terms of PI gains as well as active and reactive power setpoints. Then, all physical testing scenarios were simulated in MATLAB/Simulink, with a time-step of 100 μs, in order to compare the resulting output of the PV inverter model with those collected during the testing of the real inverter. Effectively, a portion of the experimental data were used to tune the model while all the experimental data were used for validation purposes.

A. Average PV inverter model

The assembly of an average inverter model requires the injection of AC current set-points shaped by the associated control scheme to a three-phase current source. This differs from the logic of a detailed model which would require the implementation and control of semiconductor switching (i.e. IGBTs, MOSFET). An average dynamic model is convenient for simulations of power system dynamics and assessment of the inverter's control operation, while a detailed model would be appropriate if the priority was to evaluate the impact of grid events on the semiconductor switching [12, 43, 44].

Fig. 8 illustrates a simplified 'equivalent' circuit of the model when integrated into a simple 2-bus system. The schematic shows a current source-based average model fed by the three-phase reference current waveforms, Ipv-a, Ipv-b and Ipv-c. The PV inverter AC current output, Ipv, is produced with the aid of the inverter controllers which process the decomposed active and reactive current components, I_d and I_q. These are depicted in the vector diagram of Fig. 8. Both are used to control the active and reactive power respectively, during steady state and grid disturbance conditions.

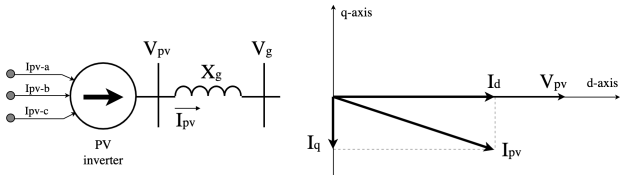

Fig. 8. Equivalent circuit of a current source representing the PV inverter connected to the grid and the output current phasor I_{pv} decoupled into active and reactive power components, I_d and I_q.

B. Control scheme

The main structure of the average PV inverter model control logic is presented in Fig. 9. It consists of three major stages:

i) the steady state and FRT 1 control part, ii) the FRT 2 and iii) the dq-abc output current transformation. The inputs of this control scheme are the active and reactive power setpoints P_{ref} and Q_{ref} as well as the measured voltage and power values V_{pv}, P_{pv} and Q_{pv}.

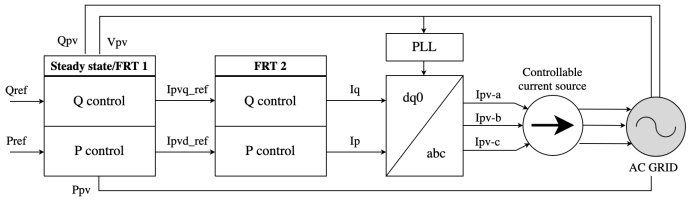

Fig. 9. Average model control structure.

1) Fault Ride Through strategy 1: FRT 1 control strategy is applied during voltage disturbances or faults, leading the inverter to increase its current output within admissible thermal limits. The P and Q control parts of first stage, depicted in Fig. 9, provide the reference values I_{pvd_ref} and I_{pvq_ref}, which form the output during steady state or FRT 1 operation. Fig. 10 introduces the particular control scheme. A PI based control loop feedback mechanism is used to continuously calculate the P and Q errors (P_{error} and Q_{error}) between the desired power set-points P_{ref}, Q_{ref} and the corresponding measured values, P_{pv} and Q_{pv}. The I_{pvd_ref} and I_{pvq_ref} are then affected by the error correction of the PI controllers and the RMS voltage at the output of the inverter. It is clarified that standard PLL, DQ0-ABC and PI blocks have been used, as the aim of this study is the replicability of the model and not the introduction of new blocks and other modelling elements.

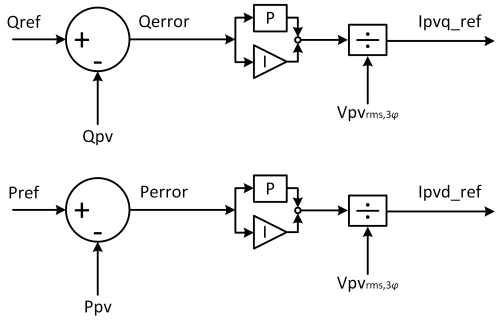

Fig. 10. Steady state control scheme.

Fig. 11 illustrates the output active and reactive power of both the inverter and the model along with the power setpoints during a network disturbance with retained voltage at 0.75 pu.

The adjustment of the FRT 1 control scheme depends on the AC voltage conditions and the loading level of the inverter. This strategy uses the steady state control architecture, presented in Fig. 10, although a number of parameters are tuned. The PI controller variables, K_p and T_i, the upper and lower PI limits (P_{upper}, Q_{upper}, P_{lower}, Q_{lower}) and other parameters such as the P and Q reference values (P_{ref} and Q_{ref}) are adaptive to the various loading levels of the inverter as well as the AC voltage RMS conditions. Tables IV, V, VI and VII list the aforementioned conditions and variables.

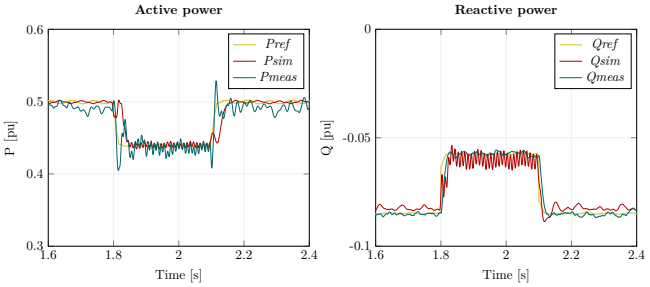

Fig. 11. Inverter active and reactive power output: 50% Loading - 0.75 pu retained voltage - FRT 1.

TABLE IV
FRT 1 - K_P PARAMETERS

Vrms (pu)	0	0.1	0.3	0.4	0.6	0.9	1.0	1.1
Kp	0.6	0.6	0.5	0.5	0.5	2.0	2.0	1.0

TABLE V
FRT 1 - T_I PARAMETERS

Loading	**T_i**
25%	0.0033
50%	0.0011
75%	0.0011
100%	0.0011

TABLE VI
FRT 1 - PI UPPER/LOWER LIMITS (pu)

Loading	**V_{rms}**	**P_{upper}**	**Q_{upper}**	**P_{lower}**	**Q_{lower}**
100%	0 - 0.8	8	0.8	-8	-0.8
	0.9 - 1	10	1	-10	-1
75%	0 - 0.8	7	0.7	-7	-0.7
	0.9 - 1	10	1	-10	-1
50%	0 - 0.8	8	0.8	-8	-0.8
	0.9 - 1	10	1	-10	-1
25%	0 - 1	8	0.04	-8	-0.04

TABLE VII
FRT 1 - ACTIVE/REACTIVE POWER SETPOINTS (pu)

Loading	**V_{rms}**	**P_{ref}**	**Q_{ref}**
100%	0	0	0
	0.8	0.7	0.875
	0.9	1	0.125
	1	1	0.125
75%	0	0	0
	0.29	0	0
	0.3	0.7	0.875
	0.4	0.8	0.1
	0.6	1	0.125
	1	1	0.125
50%	0	0	0
	0.29	0	0
	0.3	0.6	0.75
	0.5	0.8	0.1
	1	1	0.125
25%	0	1	0.125
	1	1	0.125

2) Fault Ride Through strategy 2: FRT 2 strategy is activated in case certain AC voltage thresholds are exceeded during a grid side event. The main characteristic of the FRT 2 strategy is that the PV inverter immediately stops feeding in current during the voltage disturbance or fault.

The observations captured during physical testing revealed the specific parameters and corresponding thresholds initiating the FRT 2 operation mode.

Table VIII contains the AC voltage network conditions triggering FRT 2 operation mode. In addition to the output current depression to zero during the event, gradual recovery is performed by the model after the disturbance clearance. The network parameters determining the activation of FRT 2 are the three-phase RMS voltage ($V_{3\phi}$), the single-phase RMS voltage ($V_{1\phi}$) and the voltage unbalance (V_2/V_1) [45]:

- $V_{3\phi}$: This parameter refers to the minimum threshold of the three-phase voltage RMS calculated using equation (1):

$$V_{rms,3\phi_{(pu)}} = \frac{1}{3}({V_{AB_{(pu)}}}^2 + {V_{BC_{(pu)}}}^2 + {V_{CA_{(pu)}}}^2) \quad (1)$$

- $V_{1\phi}$ and $V_{3\phi}$: FRT 2 operation is triggered when both parameters are lower than the pre-defined limits.
- V_2/V_1 and $V_{3\phi}$: The level of voltage unbalance observed at the output of the inverter is quantified using the negative to positive sequence components ratio [45]. Similar to the previous condition, the three-phase RMS voltage is also taken into account for the FRT 2 activation.

TABLE VIII
AC VOLTAGE NETWORK CONDITIONS ACTIVATING FRT 2

PV inverter loading level:	25%	50%	75%	100%
$V_{3\phi}$ [pu] $\leq$	0.05	0.29	0.3	0.65
$V_{1\phi}$ [pu] $<$ $V_{3\phi}$ [pu] $\leq$	N/A	N/A	0.15 0.69	0.15 0.81
$V_2/V_1 >$ $V_{3\phi}$ [pu] $\leq$	N/A	N/A	0.8 0.6	0.3 0.9

According to Table VIII, the activation of FRT 2, highly depends on both the AC network conditions and the loading level of the PV inverter. For instance, when the PV inverter is loaded at 50% of its nominal capacity, FRT 2 is initiated if the three-phase RMS voltage, $V_{rms,3\phi}$, is less than or equal to 0.29 pu. On the other hand, when the PV inverter is 100% loaded, the FRT 2 control part is triggered if any of the three conditions listed in the last column of Table VIII are met.

Hence, depending on the grid conditions, the $\mathbf{I_d}$ and I_q components imported in the dq0-abc block are generated either by the steady state control scheme, which matches this of the FRT 1, (depicted in Fig. 10) or by the FRT 2. Eventually, the referred time-domain current direct and quadrature (d-q axis) components are fed to the Inverse Park Transform block, as shown in Fig. 9. The latter converts I_d and I_q to a three-phase system in an a-b-c reference frame. The dq0-abc block uses equation (2) to generate the PV inverter's three-phase current output.

$$\begin{bmatrix} a \\ b \\ c \end{bmatrix} = \begin{bmatrix} \sin(\theta) & \cos(\theta) & 1 \\ \sin(\theta - \frac{2\pi}{3}) & \cos(\theta - \frac{2\pi}{3}) & 1 \\ \sin(\theta - \frac{2\pi}{3}) & \cos(\theta - \frac{2\pi}{3}) & 1 \end{bmatrix} \begin{bmatrix} d \\ q \\ 0 \end{bmatrix} \quad (2)$$

C. PV inverter model validation

The successful operation of the developed model was validated by comparing the simulation results with the measurements extracted during the physical examination of the real PV inverter. For the same purpose, the AC voltage measurements captured during testing are applied at the grid side with the aid of an emulated voltage source. The green and red colored curves in Fig. 12 - Fig. 17, present the output RMS current of the simulation model and the DUT to better visualize and compare the performance of the model against the output of the real PV inverter during the imposed grid disturbances.

The first example scenarios are used to highlight the impact of the PV inverter's loading level to the FRT response. In this case, the voltage disturbance scenarios were artificially applied by the ideal voltage source model created in RSCAD. Fig. 12 and Fig. 13 show the varying behaviors of the inverter during a 0.5 pu balanced retained voltage event when this is 25% and 75% loaded respectively. It is observed that the inverter activates FRT 1 strategy when lightly loaded, whereas it follows FRT 2 when loaded by 75% of its nominal rating. The model successfully switches from steady state to FRT 1 and FRT 2 operation mode depending on the voltage conditions seen at its output.

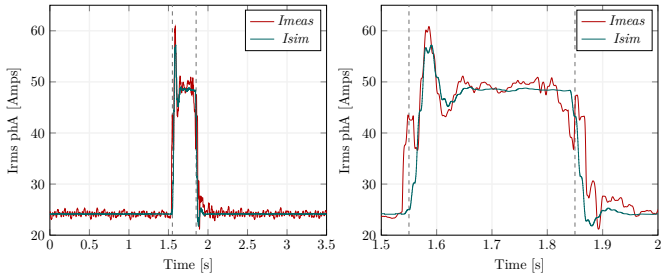

Fig. 12. Inverter output current: 25% Loading – 0.5 pu retained balanced voltage – FRT 1

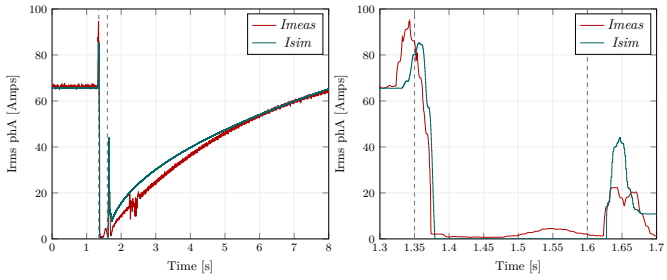

Fig. 13. Inverter output current: 75% Loading – 0.5 pu retained balanced voltage – FRT 2

The current spikes observed at the output of the inverter are emanating from the dynamic adjustment of Kp and Ti gains, transitioning from steady state rates to FRT (due to the model parametrization) and vice versa. It shall be highlighted that most of the control structures within commercial converters are not accessible, and therefore any corrective measure (e.g. bump-less transfer) cannot be directly applied (unless it is integrated by the manufacturer). However, since this study focuses primarily on the dynamic features of the model, any transient phenomena of such kind are considered out of scope.

In Fig. 14, the PV inverter activates the FRT 1 operation mode when a phase-to-ground resistive fault is applied at

location F_1 of the simulated network (Fig. 3). A 4 Amps average deviation is noted within the fault period time window of 0.4 s marked with the vertical dashed lines. The physical response of the real inverter does not seem stable in this case and differs from the current output of the inverter model which follows the FRT 1 strategy as expected. This is an outlier in the data-set which could be caused by the presence of parasitic elements arising due to the inverter's physical components or potential unforeseen experimental conditions. Moreover, an important fact taken into account while tuning the model was the consistency of its behavior across the various scenarios, which is based on this of the real inverter. Therefore, it would not be reasonable to change the control logic of the model because of one out-of-scale response. On the other hand, repetition of the experiments can nulify "unforeseen" scenarios, although this would be unfeasible in terms of time and cost. However, this mismatch explains that there is no 100 % emulation of a real PV inverter due to the hardware nature of the equipment. The reported error (4 Amps) is the largest error observed at the output of the model across the total of the applied scenarios.

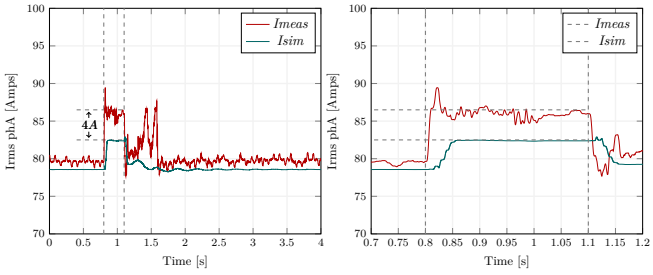

Fig. 14. Inverter output current: 100% Loading – Fault response test (phase-to-ground, fault location 1 0^o PoW, 0.1 Ω) - FRT 1.

In Fig. 15, the dynamic model matches closely the output of the real inverter. The testing scenario applies a solid fault initiated at 90^o PoW, at the same fault location as the previous case which leads the PV inverter to FRT 2 operation. The two main stages of the FRT 2 strategy can be distinguished in the graph in Fig. 15. First, the output current decreases significantly to near zero values during the event period. Secondly, when the fault clears a gradual increase of the current follows as the inverter attempts to recover the pre-fault output levels. It is observed that the RMS current curve generated by the model is very similar to that of the real device. The current spike at 1.5 sec happens instantly before the gradual "recovery" of the inverter is initiated, without exceeding any unwanted overcurrent limits.

Fig. 16 and Fig. 17 indicate how the FRT operation mode of the inverter is affected by fault location. In the former case, a fault (F_1 depicted at Fig. 3) is introduced close to the connection point of the PV inverter. This leads to a severe voltage drop at the output of the device and thus, FRT 2 is activated. On the other hand, a fault at location F_2 increases the impedance between the source (PV) and the fault. Therefore for the same type of fault to the previous case a smaller voltage dip is expected. Fig. 16 shows that, FRT 1 operation mode is

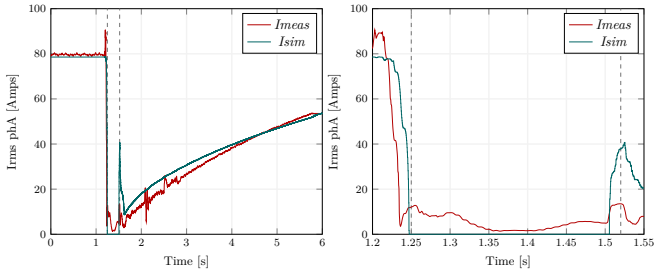

Fig. 15. Inverter output current: 100% Loading – Fault response test (phase-to-ground, fault location 1, 90^o PoW, 0 Ω) - FRT 2.

triggered by the inverter maintaining its connection stability. The model behaves in a satisfactory manner enabling both FRT 1 and FRT 2 strategies correctly, depending on the imposed AC voltage conditions.

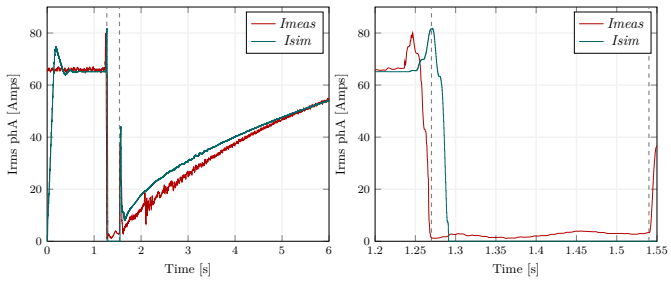

Fig. 16. Inverter output current: 75% Loading – Fault response test (phase-to-phase-to-ground, fault location 1, 0^o PoW, 0.1 Ω) - FRT 2.

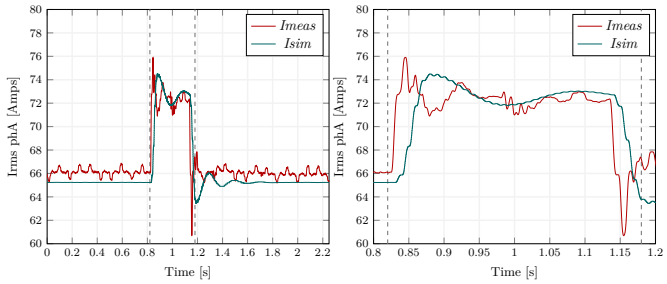

Fig. 17. Inverter output current: 75% Loading – Fault response test (phase-to-phase-to-ground, fault location 2, 0^o PoW, 0.1 Ω) - FRT 1.

The convergence of simulation and physical testing data and thus the inverter emulation accuracy is quantified with aid of the coefficient R-squared expressed by Eq. 3. The equation utilizes the measurement data y, the model response $\hat{y}$ and the mean value $\overline{y}$:

$$R - squared = 1 - \frac{\sum(y - \hat{y})^2}{\sum(y - \overline{y})^2} \tag{3}$$

The R-squared is used to show the degree of similarity between the simulation results and the target data (response of real inverter). R-squared close to 1 implies that the simulation results are very similar to the physical testing data. The R-squared values calculated for scenarios of Fig. 12 and Fig. 13, which were chosen as two representative examples of this study, are equal to 0.938 and 0.976. The above shows that the model performed with high accuracy for the referred scenarios.

D. PV inverter model network integration

The developed model is integrated in a distribution network, depicted in Fig. 18, which is also built in MATLAB Simulink. The particular work aims to characterize the profile of a network dominated by PV inverters of the tested type, when MV (11 kV) faults occur. Numerous PV systems are connected at the LV side of the grid covering 85.3% of the total demand. The 60 kVA inverter model is the grid interface of the mentioned PVs, operating in various loading levels ranging from 25% to 100% of its nominal capacity.

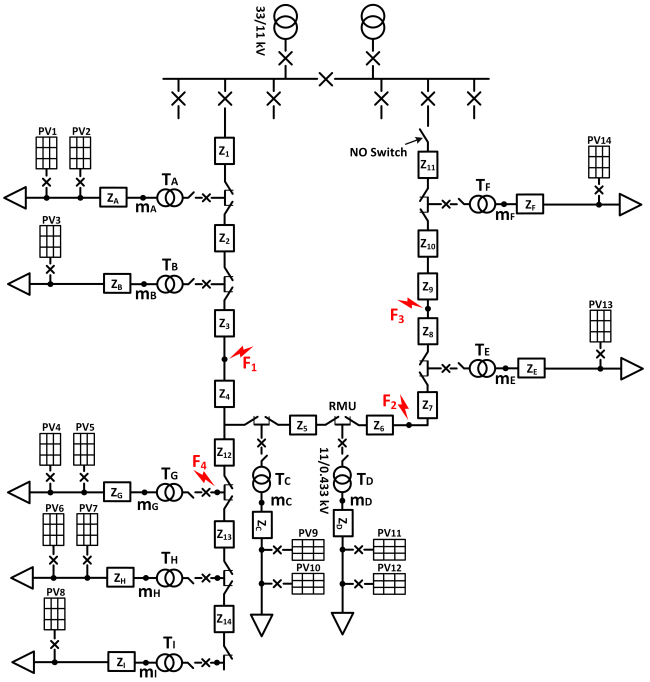

Fig. 18. Simulated network with multiple PVs.

Asymmetrical phase-to-ground and phase-to-phase faults have been introduced at the illustrated (Fig. 18) locations of the MV network, F_1 to F_4. Throughout the study, the FRT responses of the PV inverters are recorded. According to the observations acquired during the laboratory assessment of the real PV inverter, it is anticipated that the FRT outcome depends on the loading level and the network location where each emulated inverter is connected.

The parameters affecting the FRT response of the examined inverter have been reported in Table IX. These were measured at the output of each inverter model during solid (0 Ω) phase-to-phase faults applied at locations F_1 - F_4. The yellow and cyan background color of the cells denote the FRT 1 and FRT 2 operation of the corresponding inverter, respectively.

The tracked measurements logged in Table IX reveal the conditions under the PV inverters operated with one of the two fault ride-through strategies. It is inferred that FRT 2 strategy was triggered only when the thresholds defined, according to the loading level of the device, in Table VIII of Section III-B2 were exceeded. For instance, the inverter of PV_4, which operates at 100% of its capacity, performed FRT 2 during a fault at location F_1. This is because the parameters $V_{3\phi}$, V_2/V_1 and $V_{1\phi}$ exceeded the relevant predetermined thresholds during the fault. In particular the ratio V_2/V_1 was measured at 0.827 which is higher than the limit of 0.3. In addition, $V_{1\phi}$ was measured at 0.095 p.u. which combined with the $V_{3\phi}$ of 0.218 p.u. surpassing the threshold of 0.9 pu, led the inverter to FRT 2 operation.

TABLE IX
NETWORK CONDITIONS AND PV INVERTER FRT RESPONSES
PHASE TO PHASE (0 Ω) FAULT

PV inverter	Loading level	Network conditions	Fault location			
			F_1	F_2	F_3	F_4
PV_1	100%	$V_{3\phi}$ [pu]	0.421	0.804	0.874	0.495
		$V_{1\phi}$ [pu]	0.44	0.832	0.887	0.533
		V_2/V_1	0.278	0.047	0.027	0.207
PV_2	25%	$V_{3\phi}$ [pu]	0.421	0.804	0.874	0.495
		$V_{1\phi}$ [pu]	0.44	0.832	0.887	0.533
		V_2/V_1	0.278	0.047	0.027	0.207
PV_3	75%	$V_{3\phi}$ [pu]	0.223	0.739	0.84	0.326
		$V_{1\phi}$ [pu]	0.061	0.751	0.835	0.268
		V_2/V_1	0.832	0.085	0.047	0.463
PV_4	100%	$V_{3\phi}$ [pu]	0.218	0.682	0.802	0.218
		$V_{1\phi}$ [pu]	0.095	0.71	0.816	0.095
		V_2/V_1	0.827	0.109	0.057	0.828
PV_5	25%	$V_{3\phi}$ [pu]	0.218	0.682	0.802	0.218
		$V_{1\phi}$ [pu]	0.095	0.71	0.816	0.095
		V_2/V_1	0.827	0.109	0.057	0.828
PV_6	100%	$V_{3\phi}$ [pu]	0.193	0.681	0.797	0.193
		$V_{1\phi}$ [pu]	0.018	0.802	0.802	0.018
		V_2/V_1	1.002	0.109	0.057	0.
PV_7	50%	$V_{3\phi}$ [pu]	0.193	0.681	0.797	1.003
		$V_{1\phi}$ [pu]	0.018	0.802	0.802	0.018
		V_2/V_1	1.002	0.109	0.057	1.003
PV_8	50%	$V_{3\phi}$ [pu]	0.211	0.662	0.787	0.211
		$V_{1\phi}$ [pu]	0.144	0.703	0.817	0.012
		V_2/V_1	1	0.117	0.062	1.001
PV_9	100%	$V_{3\phi}$ [pu]	0.212	0.687	0.809	0.221
		$V_{1\phi}$ [pu]	0.144	0.708	0.812	0.147
		V_2/V_1	0.802	0.109	0.057	0.748
PV_{10}	25%	$V_{3\phi}$ [pu]	0.211	0.684	0.805	0.22
		$V_{1\phi}$ [pu]	0.144	0.708	0.812	0.147
		V_2/V_1	0.802	0.109	0.057	0.748
PV_{11}	25%	$V_{3\phi}$ [pu]	0.815	0.77	0.955	0.335
		$V_{1\phi}$ [pu]	0.202	0.77	0.9	0.175
		V_2/V_1	0.782	0.122	0.064	0.726
PV_{12}	50%	$V_{3\phi}$ [pu]	0.314	0.818	0.96	0.337
		$V_{1\phi}$ [pu]	0.202	0.77	0.9	0.175
		V_2/V_1	0.782	0.122	0.064	0.726
PV_{13}	50%	$V_{3\phi}$ [pu]	0.207	0.208	0.21	0.214
		$V_{1\phi}$ [pu]	0.014	0.014	0.019	0.031
		V_2/V_1	1	1.001	0.967	0.917
PV_{14}	50%	$V_{3\phi}$ [pu]	0.207	0.22	0.22	0.227
		$V_{1\phi}$ [pu]	0.004	0.22	0.003	0.03
		V_2/V_1	0.999	1	1	0.916

Table IX presents a significant variation of the resulting FRT operation modes. Specifically, 64.28% of the inverters activate FRT 2 during a fault at location F_1. This means that 330 kVA of distributed generation is depressed to zero during the fault period of this scenario. Similarly, the 57.14% of the total PV generation switched to FRT 2 mode during a phase-to-phase fault at location F_4. On the other hand, the referred percentage dropped to 14.3% during the F_2 and F_3 scenarios.

In addition, Table IX shows that the observed discrepancy in terms of FRT response among the numerous PV inverters of the same type is highly dependent on the fault location and the loading level of the device. The latter can be affected by the regional weather conditions (i.e. solar irradiance, am-

bient temperature), the solar panels capacity, the level of PV modules shading, etc.

The noted variation of inverter behavior during fault conditions is expected to increase when PV inverters of different manufacturers are connected to the network. The mentioned uncertainty challenges network planning with regards to the decision of equipment thermal limits, the calculation of fault current levels and the design of protection schemes. Future work assessing the performance of the developed configurable model while emulating additional types of PV inverters is considered of high importance.

IV. Conclusions

The paper has presented a methodology and a corresponding dynamic model which can be deployed for the emulation and hardware validation of small scale PV inverters of various manufacturers. In this study, the utilized model was tuned in order to emulate the fault response of a particular commercially available PV inverter. The validation of the model was based on the experimental characterization of a 60 kVA LV PV inverter response under varied short circuit and voltage depression testing conditions. The tests involved depression of the AC voltage across the inverter output - directly or indirectly via faults - for different loading levels ranging from 25% to 100%.

A significant remark noted throughout physical testing was the identification of the diverse FRT responses along with their distinct stages. The inverter under test exhibited two types of fault ride through strategies when voltage disturbances and fault conditions were applied at the AC network. The one resulted in a slight increase in the output current of the inverter and it was enabled under certain network conditions. The second strategy was activated when predefined thresholds were exceeded. The output current is depressed to near zero values followed by a gradual recovery just after the end of the event (fault clearance, grid voltage recovery).

The observations reported during the simulations, where a vast amount of PVs interfaced the grid via the developed inverter model, revealed a significant variance of responses when faults were applied. It can be assumed that the problem can be further magnified when inverters of different manufacturers are connected to the system. Consequently, there is a value in deploying the presented adjustable inverter model as its parameters can be tuned to represent various inverter types. The use of a configurable model, which could potentially be tuned in an automatic way via an algorithmic process, would benefit larger power system studies performed by the DSOs, assessing the effect of small scale PV inverters penetration to the distribution networks in a more reliable manner.

References

[1] Committee on Climate Change, "Net Zero – The UK's contribution to stopping global warming." [Online]. Available: https://bit.ly/2OhMCHf

[2] I. Abdulhadi and A. Dyśko, "Hardware testing of photovoltaic inverter loss of mains protection performance," in *13th International Conference on Development in Power System Protection 2016 (DPSP)*, 2016, pp. 1–6.

[3] I. Abdulhadi, F. Coffele, A. Dyśko, C. Foote, C. Kungu, and M. Lee, "Hardware-based characterisation of lv inverter fault response," *CIRED - Open Access Proceedings Journal*, vol. 2017, no. 1, pp. 1167–1171, 2017.

[4] L. Callegaro, G. Konstantinou, C. A. Rojas, N. F. Avila, and J. E. Fletcher, "Testing evidence and analysis of rooftop pv inverters response to grid disturbances," *IEEE Journal of Photovoltaics*, vol. 10, no. 6, pp. 1882–1891, 2020.

[5] P. Bountouris, I. Abdulhadi, A. Dysco, and F. Coffele, "Characterising grid connection stability of low voltage pv inverters through real-time hardware testing," pp. 1–5, June 2019.

[6] B. Popadic, B. Dumnic, and L. Strezoski, "Modeling of initial fault response of inverter-based distributed energy resources for future power system planning," *International Journal of Electrical Power and Energy Systems*, vol. 117, p. 105722, 2020.

[7] J. Alvidrez, S. Ranade, S. Brahma, S. Bukowski, C. Silva-Monroy, and A. Ellis, "An analytical model of a single phase DQ-controlled inverter for power system short circuit calculations," in *2016 North American Power Symposium (NAPS)*, 2016, pp. 1–5.

[8] D. J. Rincón, M. A. Mantilla, J. M. Rey, and M. Garnica, "Dc stage modelling for lvrt capability in photovoltaic systems," in *IECON 2021 – 47th Annual Conference of the IEEE Industrial Electronics Society*, 2021, pp. 1–7.

[9] L. Sigrist, J. Renedo, F. M. Echavarren, F. P. Thoden, and L. Rouco, "Modeling of steady state fault current contribution of inverter-connected generation in pss/e," in *2021 IEEE Madrid PowerTech*, 2021, pp. 1–6.

[10] X. Shi, H. Zhang, C. Wei, Z. Li, and S. Chen, "Fault modeling of iidg considering inverter's detailed characteristics," *IEEE Access*, vol. 8, pp. 183 401–183 410, 2020.

[11] L. Wang, T. Qiao, B. Zhao, and X. Zeng, "Modeling and parameter identification of grid-connected pv system during asymmetrical grid faults," in *2019 IEEE 3rd Conference on Energy Internet and Energy System Integration (EI2)*, 2019, pp. 2086–2090.

[12] A. Ekic, M. Maharjan, B. Strombeck, and D. Wu, "Impact of inverter modeling on sub-cycle dynamics in grid-connected solar pv systems," in *2021 IEEE 48th Photovoltaic Specialists Conference (PVSC)*, 2021, pp. 1173–1175.

[13] C. A. Plet, M. Brucoli, J. D. F. McDonald, and T. C. Green, "Fault models of inverter-interfaced distributed generators: Experimental verification and application to fault analysis," in *2011 IEEE Power and Energy Society General Meeting*, 2011, pp. 1–8.

[14] I. Abdulhadi, F. Coffele, A. Dysko, C. Foote, and C. Kungu, "Hardware-based characterisation of lv inverter fault response," 2017, p. 1167 – 1171.

[15] C. A. Plet, M. Graovac, T. C. Green, and R. Iravani, "Fault response of grid-connected inverter dominated networks," in *IEEE PES General Meeting*, 2010, pp. 1–8.

[16] E. Muljadi, M. Singh, R. Bravo, and V. Gevorgian, "Dynamic model validation of pv inverters under short-circuit conditions," in *2013 IEEE Green Technologies Conference (GreenTech)*, 2013, pp. 98–104.

[17] R. J. Bravo, R. Yinger, and S. Robles, "Three phase solar photovoltaic inverter testing," in *2013 IEEE Power Energy Society General Meeting*, 2013, pp. 1–5.

[18] T. Ivanov and R. Stanev, "Mathematical model of photovoltaic inverters," in *2019 11th Electrical Engineering Faculty Conference (BulEF)*, 2019, pp. 1–5.

[19] J. Hernandez-Alvidrez, A. Summers, N. Pragallapati, M. J. Reno, S. Ranade, J. Johnson, S. Brahma, and J. Quiroz, "PV-Inverter Dynamic Model Validation and Comparison Under Fault Scenarios Using a Power Hardware-in-the-Loop Testbed," in *2018 IEEE 7th World Conference on Photovoltaic Energy Conversion (WCPEC) (A Joint Conference of 45th IEEE PVSC, 28th PVSEC 34th EU PVSEC)*, 2018, pp. 1412–1417.

[20] N. Ninad, D. Turcotte, and T. EL-Fouly, "Grid-interactive inverter modeling for power system studies," in *2015 IEEE Power Energy Society General Meeting*, 2015, pp. 1–5.

[21] R. Mahmud, A. Hoke, and D. Narang, "Fault response of distributed energy resources considering the requirements of ieee 1547-2018," in *2020 IEEE Power Energy Society General Meeting (PESGM)*, 2020, pp. 1–5.

[22] A. Ekic, M. Maharjan, B. Strombeck, and D. Wu, "Impact of inverter modeling on sub-cycle dynamics in grid-connected solar pv systems," in *2021 IEEE 48th Photovoltaic Specialists Conference (PVSC)*, 2021, pp. 1173–1175.

[23] M. Patel, "Opportunities for standardizing response, modeling and analysis of inverter-based resources for short circuit studies," *IEEE Transactions on Power Delivery*, vol. 36, no. 4, pp. 2408–2415, 2021.

[24] H. Satoh, K. Yamashita, K. Shirasaki, and Y. Kitauchi, "Root-mean square model of three-phase photovoltaic inverter for unbalanced fault," in *2021 IEEE Power Energy Society General Meeting (PESGM)*, 2021, pp. 01–01.

[25] Kara Clark, Nicholas W. Miller, Reigh Walling, "Modeling of GE solar photovoltaic plants for grid studies," April 2016.

[26] Electric Power Research Institute (EPRI), "Technical update on generic wind and solar PV model development and validation," 2014.

[27] Western Electricity Coordinating Council, "Generic solar photovoltaic system dynamic simulation model specification," 2012.

[28] W. E. C. Council, "WECC solar plant dynamic modelling guidelines," 2014.

[29] C. D. Booth, F. Coffele, and G. M. Burt, "The power networks demonstration centre: An environment for accelerated testing, demonstration and validation of existing and novel protection and automation systems," in *12th IET International Conference on Developments in Power System Protection (DPSP 2014)*, March 2014, pp. 1–6.

[30] I. R. S. Priyamvada and S. Das, "Adaptive tuning of pv generator control to improve stability constrained power transfer capability limit," *IEEE Transactions on Power Systems*, pp. 1–1, 2021.

[31] L. M. Kandasamy, J. Kanakaraj, and S. J, "Artificial neural network based intelligent controller design for grid-tied inverters of microgrid under load variation and disturbance," in *2021 4th International Conference on Recent Developments in Control, Automation Power Engineering (RDCAPE)*, 2021, pp. 148–153.

[32] Energy Networks Association, "ER G83/2: Recommendations for the connection of type tested small-scale embedded generators (up to 16a per phase) in parallel with low-voltage distribution systems." 2012.

[33] National Grid Electricity Transmission, "The Grid Code - Issue 5," 03 2017.

[34] "RTDS, "Real Time Digital Power System Simulator, RTDS Technologies Inc," https://www.rtds.com/, accessed: 2020-02-09.

[35] Triphase, "Programmable Power Conversion for RnD and Education," https://triphase.com/, accessed: 2020-02-09.

[36] ETPS, "Grid-tied bidirectional DC supply," https://bit.ly/3nOMP3X, accessed: 2020-11-06.

[37] Beckhoff. EL3773 power monitoring oversampling terminal. [Online]. Available: https://goo.gl/9pa2V4

[38] N. Hatziargyriou, J. Milanovic, C. Rahmann, V. Ajjarapu, C. Canizares, I. Erlich, D. Hill, I. Hiskens, I. Kamwa, B. Pal, P. Pourbeik, J. Sanchez-Gasca, A. Stankovic, T. Van Cutsem, V. Vittal, and C. Vournas, "Definition and classification of power system stability – revisited amp; extended," *IEEE Transactions on Power Systems*, vol. 36, no. 4, pp. 3271–3281, 2021.

[39] ——, "Stability definitions and characterization of dynamic behavior in systems with high penetration of power electronic interfaced technologies," *Power System Dynamic Performance Committee (PSDP)*, 2020.

[40] ENWL, "Low Voltage Network Solutions (LVNS)," https://bit.ly/3BtJ7V4, accessed: 2020-11-06.

[41] F. Blaabjerg, R. Teodorescu, M. Liserre, and A. Timbus, "Overview of control and grid synchronization for distributed power generation systems," *IEEE Transactions on Industrial Electronics*, vol. 53, no. 5, pp. 1398–1409, 2006.

[42] S. Ma, H. Geng, L. Liu, G. Yang, and B. C. Pal, "Grid-synchronization stability improvement of large scale wind farm during severe grid fault," *IEEE Transactions on Power Systems*, vol. 33, no. 1, pp. 216–226, 2018.

[43] A. Ellis, M. R. Behnke, and R. T. Elliott, "Generic solar photovoltaic system dynamic simulation model specification," https://www.osti.gov/servlets/purl/1177082, 2013.

[44] Z. Jankovic, B. Novakovic, V. Bhavaraju, and A. Nasiri, "Average modeling of a three-phase inverter for integration in a microgrid," in *2014 IEEE Energy Conversion Congress and Exposition (ECCE)*, 2014, pp. 793–799.

[45] F. Ghassemi and M. Perry, "Review of Voltage Unbalance Limit in The GB Grid Code CC.6.1.5 (b)," p. 35, 10 2014.